Electronic-structure calculations, photoelectron spectra, optical spectra, and Mössbauer parameters for the pyrites MS_2 (M=Fe, Co, Ni, Cu, Zn)

S. Lauer and A. X. Trautwein
Institut für Physik, Medizinische Hochschule, D-2400 Lübeck 1, Federal Republic of Germany

F. E. Harris
Department of Physics, University of Utah, Salt Lake City, Utah 84112
(Received 22 November 1983)

Electronic-structure calculations on the basis of a self-consistent charge, linear combination of atomic orbitals band-structure method have been performed for the pyrites FeS_2, CoS_2, NiS_2, CuS_2, and ZnS_2. Photoelectron spectra, optical spectra, and Mössbauer parameters are evaluated and are found to compare well with experimental data. Molecular-orbital cluster calculations have been performed to derive local properties (Mössbauer parameters) only, which are compared with band-structure and experimental results. Clusters which include S_2 anion pairs, i.e., $[M(S_2)_6]^{10-}$, yield reasonable results, while for the smaller clusters $[MS_6]^{4-}$, even convergence could not be achieved. Our further investigation includes (i) the pressure dependence of ΔE_Q and δ in FeS_2; (ii) the concentration dependence of ΔE_Q in the solid solutions $Fe_xCo_{1-x}S_2$ (x=0.01,0.25,0.5,0.75); (iii) the sign of the nuclear-quadrupole coupling constant e^2qQ, which was found to be negative except for ZnS_2; (iv) the various contributions to the electric-field gradient (EFG) tensor (in FeS_2 the main contribution arises from the valence shell, and proceeding from FeS_2 to ZnS_2 in the pyrite series, the valence contribution continuously decreases, and in the d^{10} system ZnS_2 only a small and positive lattice EFG is left); (v) the interpretation of the independence of the Mössbauer line intensity ratio from the single-crystal orientation with respect to the γ beam on the basis of our calculated EFG tensor.

I. INTRODUCTION

There has been considerable interest in the electronic structure of the transition-metal dichalcogenides because of their wide range of electric, magnetic, and optical properties.[1] During the last few years many experimental studies have been reported on the transition-metal disulfides MS_2 (M=Fe, Co, Ni, Cu, Zn) with the pyrite structure: Photoelectron spectroscopy has been used[2–7] to study the core and valence-band levels of the MS_2 series. Optical experiments have been performed[8–11] to gain information about the empty electronic states. With the help of Mössbauer spectroscopy the local electronic structure at the iron site in FeS_2,[12–23] and iron-doped CoS_2[16,17,20,24,25] and NiS_2,[20,25,26] was investigated.

Theoretical work has been performed on the basis of the self-consistent-field (SCF) $X\alpha$ cluster method,[3,27,28] but no effort has been undertaken to evaluate expectation values. Further theoretical work[29,30] has been performed on the basis of the linear combination of atomic orbitals (LCAO) tight-binding (TB) band-structure method. Khan[29] has used the non-self-consistent LCAO TB method for the calculation of the band structure in FeS_2. Bullett[30] evaluated, with a partially self-consistent scheme, the band structure and the density of states for the entire MS_2 series. However, both focused their interest on the density of states only. In this paper we want to present a comprehensive study of the electronic structure of the MS_2 series by using self-consistent molecular-orbital (MO) cluster and band-structure calculations. Photoelectron spectra and the imaginary part of the dielectric constant as well as the local Mössbauer parameters are evaluated. In Sec. II we shall describe the principles of the methods, and in Sec. III we present and discuss our results.

II. CALCULATIONAL PROCEDURE

A. Theoretical model

In the LCAO TB method a crystal wave function or band $|\mu,\vec{k};\vec{r}\rangle$ with wave vector $\vec{k}$ and spatial coordinate $\vec{r}$ is represented as a linear combination of Bloch basis orbitals $|i,\vec{k};\vec{r}\rangle$,

$$|\mu,\vec{k};\vec{r}\rangle=\sum_i c_{i\mu}(\vec{k})\,|i,\vec{k};\vec{r}\rangle\ . \tag{1}$$

The Bloch functions $|i,\vec{k};\vec{r}\rangle$ are constructed by a superposition of equivalent atomic orbitals (AO's) $|i;\vec{R}_l\rangle$, which are centered in the unit cells labeled by the direct lattice vectors $\vec{R}_l$,

$$|i,\vec{k};\vec{r}\rangle=\frac{1}{(N_c)^{1/2}}\sum_l e^{i\vec{k}\cdot\vec{R}_l}\,|i;\vec{R}_l\rangle\ . \tag{2}$$

N_c denotes the number of unit cells in the summation. The atomic orbitals $|i;\vec{R}_l\rangle$ used in this investigation are Slater-type orbitals (STO's) with screening constant ζ. The one-electron Schrödinger equation, which may describe the electronic structure of the many-particle system, is (in a.u.)

$$[-\nabla^2+V(\vec{r})]\,|\mu,\vec{k};\vec{r}\rangle=E_\mu(\vec{k})\,|\mu,\vec{k};\vec{r}\rangle\ , \tag{3}$$

where $V(\vec{r})$ refers to the periodic crystal potential. Multiplying Eq. (3) with the Bloch function $|j,\vec{k};\vec{r}\rangle$ and integrating over the electronic coordinates, we obtain the secular equation

$$\sum_i [H_{ij}(\vec{k})-E_\mu(\vec{k})S_{ij}(\vec{k})]c_{i\mu}(\vec{k})=0 , \tag{4}$$

where $S_{ij}(\vec{k})$ is the overlap matrix between Bloch functions

$$S_{ij}(\vec{k})=\sum_l e^{i\vec{k}\cdot\vec{R}_l}\langle i;\vec{R}_0|j;\vec{R}_l\rangle = \sum_l e^{i\vec{k}\cdot\vec{R}_l}S_{ij}(\vec{R}_l) . \tag{5}$$

$S_{ij}(\vec{R}_l)$ defines the overlap between AO's. $H_{ij}(\vec{k})$ is the Hamiltonian matrix,

$$H_{ij}(\vec{k})=\sum_l e^{i\vec{k}\cdot\vec{R}_l}\langle i;\vec{R}_0|-\nabla^2+V(\vec{r})|j;\vec{R}_l\rangle = \sum_l e^{i\vec{k}\cdot\vec{R}_l}h_{ij}(\vec{R}_l) . \tag{6}$$

Similar to the extended-Hückel MO Theory, the matrix elements $h_{ii}(\vec{R}_0)$ are interpreted as the ionization potential of an electron in an atomic orbital $|i\rangle$ in the solid. h_{ii} can be represented, therefore, as a sum of an atomic ionization potential I_i plus a Madelung correction M_i and higher-order crystal-field terms W_i,[31]

$$h_{ii}(\vec{R}_0)=-(I_i+M_i)+W_i . \tag{7a}$$

The off-diagonal Hamiltonian matrix elements $h_{ij}(\vec{R}_l)$ are evaluated on the basis of the Cusach's approximation,[32]

$$h_{ij}(\vec{R}_l)=\tfrac{1}{2}[2-|S_{ij}(\vec{R}_l)|]S_{ij}(\vec{R}_l)(h_{ii}+h_{jj}) \quad (i\neq j \text{ if } \vec{R}_l=\vec{R}_0) . \tag{7b}$$

Inserting Eqs. (7) into Eq. (6) yields

$$H_{ij}(\vec{k})=\tfrac{1}{2}F_{ij}(\vec{k})(h_{ii}+h_{jj}) , \tag{8}$$

with $F_{ij}(\vec{k})$ being the complex Cusachs factor matrix. The atomic ionization potential I_i of an electron in an atomic orbital $|i\rangle$ belonging to an atom with charge Q is represented as

$$I_i=\alpha_0^i+\Delta\alpha^i Q , \tag{9}$$

where α_0 and $\Delta\alpha$ can be taken from spectroscopic tables.[33] The Madelung-potential term M_i in Eq. (7a) is calculated using a recently developed direct lattice summation scheme.[34] M_i is recalculated in each iteration with the new effective charges obtained by the previous iteration. The crystal-field term W_i [Eq. (7a)] is taken as the diagonal model-potential contribution to the Hamiltonian as evaluated by Grodzicki [Eq. (9) of Ref. 35]. The zeroth-order term in the expansion of the model potential has to be excluded here because this term is already included in the Madelung potential M_i. W_i was calculated taking into account all atoms within the central and next-neighbor unit cells. In this specific model-potential approximation the atomic model potential is constructed from a spherically symmetric but exponentially decaying charge distribution. The decay is controlled by a screening constant in the form $\eta=\eta_0+\eta_1 Q$, with Q being the effective charge of this atom [Eq. (12)—(23) in Ref. 35]. Solving the Schrödinger equation provides us with band energies $E_\mu(\vec{k})$ and eigenvectors $c_{i\mu}(\vec{k})$, which then can be used to deduce the population q_i of AO's,

$$q_i=\frac{\Omega}{8\pi^3}\sum_j \int_{BZ} d^3k\, P_{ij}(\vec{k})S_{ij}(\vec{k}) . \tag{10}$$

Ω is the volume of the primitive unit cell, and the integration has to be carried out over the volume of the first Brillouin zone (BZ). The "bond-order" matrix $P_{ij}(\vec{k})$ is given as

$$P_{ij}(\vec{k})=\sum_\mu c_{j\mu}(\vec{k})n(E_\mu(\vec{k})) .$$

$n(E_\mu(\vec{k}))$ defines the occupation of the one-particle state as defined by Eq. (1), and its values range from 0 to 2. The effective atomic charges Q in the unit cell are evaluated from the orbital population number q_i. Then the Hamiltonian matrix [Eq. (8)] is reconstructed, and the secular equation is again solved until self-consistency is reached (up to $0.03e$).

The density of electronic states $D(E)$ is defined by

$$D(E)=\frac{\Omega}{8\pi^3}\sum_\mu \int_{BZ} d^3k\,\delta(E_\mu(\vec{k})-E)n(E_\mu(\vec{k})) . \tag{12}$$

A histogram sampling has been used to evaluate $D(E)$. The photoelectron intensities $I(E)$ are derived from

$$I(E)=\frac{\Omega}{8\pi^3}\sum_\mu \int_{BZ} d^3k\,\sigma_\mu(\vec{k},\omega)\delta(E_\mu(\vec{k})-E)n(E_\mu(\vec{k})) , \tag{13}$$

where $\sigma_\mu(\vec{k},\omega)$ is the transition probability from a bound state $|\mu,\vec{k};\vec{r}\rangle$ to a continuum state $|c,\omega\rangle$ with energy $\hbar\omega$.[36] $\sigma_\mu(\vec{k},\omega)$ can be represented in dipolar approximation by

$$\sigma_\mu(\vec{k},\omega)\propto|\langle\mu,\vec{k};\vec{r}|\vec{r}|c,\omega\rangle|^2 = \sum_{i,j} c_{i\mu}^*(\vec{k})c_{j\mu}(\vec{k})\sum_l e^{i\vec{k}\cdot\vec{R}_l}\sigma_{ij}(\omega) . \tag{14}$$

Here we have made use of Eqs. (1) and (2), and we have introduced the atomic photoionization cross sections $\sigma_{ij}(\omega)$. The diagonal elements $\sigma_{ii}(\omega)$ can be taken from atomic calculations[37,38] or from experimental data,[39] while for the off-diagonal elements we use the approximation

$$\sigma_{ij}(\omega)=\tfrac{1}{2}S_{ij}(\vec{R}_l)[\sigma_{ii}(\omega)+\sigma_{jj}(\omega)] . \tag{15}$$

In the actual calculation the δ function in Eq. (13) is replaced by a Gaussian of linewidth ($\beta=0.4$ eV) to simulate the spectrometer resolution,

$$\delta(E_\mu-E)\rightarrow\frac{1}{\sqrt{2\pi}\beta}\exp[-(E_\mu-E)^2/2\beta^2] .$$

In order to compare the calculated band structure with

optical data, we evaluate the imaginary part of the dielectric constant $\epsilon_2(E)$ in the dipolar approximation using the relation[40]

$$\epsilon_2(E) \propto \frac{1}{E^2} \sum_{\mu}^{\text{occ}} \sum_{\nu}^{\text{emp}} \int_{\text{BZ}} d^3k \, | Z_{\mu\nu}(\vec{k}) |^2 \times \delta(| E_{\mu}(\vec{k}) - E_{\nu}(\vec{k}) | - E) , \tag{16}$$

where $Z_{\mu\nu}(\vec{k})$ refers to the transition matrix element $\langle \mu, \vec{k}; \vec{r} \,|\, \vec{r} \,|\, \nu, \vec{k}; \vec{r} \rangle$. Proceeding in a similar fashion as in Eq. (14) the transition matrix elements can be reduced to the evaluation of dipole matrix elements between AO's,

$$Z_{\mu\nu}(\vec{k}) \propto \sum_{i,j} c^*_{i\mu}(\vec{k}) c_{j\nu}(\vec{k}) \sum_{l} e^{i\vec{k}\cdot\vec{R}_l} \langle i; \vec{R}_0 \,|\, \vec{r} \,|\, j; \vec{R}_l \rangle . \tag{17}$$

The δ function in Eq. (16) was replaced in the actual calculation by a Gaussian with linewidth $\beta = 0.1$ eV.

The calculation of the electric-field-gradient (EFG) tensor at the nuclear site of, e.g., a Mössbauer isotope consists of first dividing the total charge of the solid into the positive point charges q of the atomic cores, and then into the charge distribution of all electrons. The EFG tensor then can be represented as the sum of a core and an electronic part,

$$V_{pq} = V_{pq}^{\text{core}} + V_{pq}^{\text{el}} . \tag{18}$$

Since the core wave functions of an atom are strongly localized it is a reasonable approximation to evaluate V_{pq}^{core} on the basis of a point-charge model. The direct lattice summation scheme of Ref. 34 has been used to evaluate this contribution. V_{pq}^{el}, however, has to be calculated, in general, by direct evaluation of the proper matrix elments,

$$V_{pq}^{\text{el}} = \frac{\Omega}{8\pi^3} \int_{\text{BZ}} d^3k \sum_{\mu} n(E_{\mu}(\vec{k})) \langle \mu, \vec{k}; \vec{r} \,|\, \hat{V}_{pq}(\vec{r}) \,|\, \mu, \vec{k}; \vec{r} \rangle , \tag{19}$$

with $\hat{V}_{pq}(\vec{r})$ being the EFG-tensor operator,

$$\hat{V}_{pq}(\vec{r}) = [1 - \gamma(r)] \frac{3 r_p r_q - r^2 \delta_{pq}}{r^5} \quad (p,q = x,y,z) . \tag{20}$$

$\gamma(r)$ represents the Sternheimer shielding function[41] which describes the polarization of the frozen electronic core of the Mössbauer atom by external charges.[42] Inserting the expansions of Eq. (1) and (2) into Eq. (19) yields

$$V_{pq}^{\text{el}} = \frac{\Omega}{8\pi^3} \int_{\text{BZ}} d^3k \sum_{i,j} P_{ij}(\vec{k}) \times \sum_{l} e^{i\vec{k}\cdot\vec{R}_l} \langle i; \vec{R}_0 \,|\, \hat{V}_{pq}(\vec{r}) \,|\, j; \vec{R}_l \rangle . \tag{21}$$

The EFG-tensor matrix elements between AO's can then be evaluated with the same techniques as described by Grodzicki *et al.*[43] For further discussion, we wish to emphasize here that the usual separation of the EFG tensor into a valence part and a lattice part is only justified if the EFG contribution from the overlap charges between the Mössbauer atom and its ligands is small compared to all other contributions.

B. $\vec{k}$-space integration

If in band-structure calculations functions have to be integrated which have the full symmetry of the lattice [as in Eq. (12)], the integration is generally performed in the irreducible part of the first Brillouin zone. For these integrations we have used (a) products of one-dimensional Gauss or Chebyshev and not Gauss-Chebyshev formulas,[44] (b) the special-point approach of Monkhorst and Pack,[45] and (c) the special-direction formulas of Fehlner *et al.*[47] However, if the functions do not possess the required symmetry [as in Eq. (21)], a straightforward application of the irreducible-zone concept is not possible. In such cases the integration was performed over the entire Brillouin zone with Gauss or Chebyshev product formulas. The number of quadrature points was varied from 64 (4^3) to 2744 (14^3), but already at 64 points, stable results were obtained. Comparing the three integration schemes it turned out that the Gauss or Chebyshev product formulas are slightly more efficient than the special-point formulas. However, it should be mentioned that this statement cannot be generalized, since the efficiency of integration formulas will always depend on the function to be integrated. If the special-direction scheme with low-order integration formulas is used to calculate the density of states $D(E)$, at first only small differences with respect to the other integration formulas occur. However, if this technique is used to evaluate the photoelectron spectra, emissions are found from the e_g bands of FeS_2, although these bands should be empty. If the integration is improved by using higher-order formulas this emission diminishes and finally disappears. This result can be explained by the fact that the special-direction formulas are not normalized to the volume of the Brillouin zone: When integrating the volume of the zone, the correct value is approached from below if the accuracy of the integration is increased. For a small number of integration points, each point carries insufficient weight. Calculating photoelectron spectra, one therefore has to integrate to higher-energy terms (which actually should be empty), in order to fill in all electrons. To overcome this problem the special-direction formulas should always be normalized to the volume of the Brillouin zone.

C. Parametrization

The atomic valence orbitals $| i; R_l \rangle$ [Eq. (2)] which have been used in this investigation are $4s$, $4p$, and $3d$ orbitals for the metal atom, and $3s$ and $3p$ for sulfur. Since four metal and eight sulfur atoms belong to the primitive unit cell of the pyrites, we are concerned with a basis dimension of 68 AO's. Slater exponents ζ, ionization potential parameters α_0 and $\Delta\alpha$, as well as the model-potential parameters η_0 and η_1, are summarized in Table I. All parameters have been chosen in accordance with our previ-

TABLE I. Ionization potential parameters α_0 and $\Delta\alpha$, screening constants ζ of Slater-type orbitals, and model-potential parameters η_0 and η_1.

Atom	Orbital	α_0 (eV)	$\Delta\alpha$ (eV)	ζ (a.u.$^{-1}$)	η_0 (a.u.$^{-1}$)	η_1 (a.u.$^{-1}$)
Fe	4*s*	4.2	8.0	2.00	3.6	0.7
	4*p*	3.7	8.0	2.00		
	3*d*	7.0	8.0	2.87		
Co	4*s*	3.8	9.0	2.04	3.7	0.7
	4*p*	3.3	9.0	2.04		
	3*d*	6.9	9.0	3.10		
Ni	4*s*	3.4	10.0	2.10	3.8	0.7
	4*p*	2.9	10.0	2.10		
	3*d*	6.7	10.0	3.25		
Cu	4*s*	3.6	12.0	2.00	4.0	0.7
	4*p*	3.0	12.0	2.00		
	3*d*	6.8	12.0	3.50		
Zn	4*s*	5.4	8.0	2.20	4.0	0.7
	4*p*	4.9	8.0	2.20		
	3*d*	17.4	8.0	3.50		
S	3*s*	22.0	11.0	1.82	2.5	0.9
	3*p*	8.0	11.0	1.82		

ous molecular-orbital work,[43,48] and only a few adjustments had to be made. We have used slightly larger Slater exponents for the metal 4*s* and 4*p* AO's compared to our MO work. This contraction of wave functions in the solid state is expected to be largest for wave functions which are already extended in the free-atomic case. These findings agree with our previous band structure calculations on $BaTiO_3$.[31]

D. Structural data

The cubic pyrite structure with space group T_h^6 is a common feature of all crystals being investigated in this work. The pyrite structure can be considered as a NaCl-like lattice where the metal atom M occupies the Na position while the chlorines are replaced by S_2 pairs directing along the four $\langle 111 \rangle$ directions of the cubic unit cell. The structural data used here are identical to the one used by Bullett.[30] For the pressure-dependent calculations in the FeS_2 system the lattice parameters have been taken from Vaughan and Drickamer,[14] but in order to allow a comparison with the slightly different lattice parameters quoted by Bullett, the lattice constants have been renormalized to Bullett's zero-pressure values. A similar renormalization has been applied for the structural data in the solid solution series $Fe_xCo_{1-x}S_2$ ($x=0.01,0.25,0.5,0.75$), where the data have been reported by Gallagher *et al.*[16]

E. MO-cluster calculations

In order to allow a comparison with MO-cluster methods we additionally performed cluster calculations for the MS_2 series using a standard iterative extended-Hückel theory (IEHT) MO method.[48] For a $[MS_6]^{4-}$ cluster we have not been able to arrive at a meaningful converged result. In FeS_2 this arises because the energy splitting between occupied t_{2g} and empty e_g levels is too small. We have therefore extended the cluster by including S_2 pairs, thus yielding a $[M(S_2)_6]^{10-}$ cluster. Based on such clusters, we have calculated, according to the methods described in Refs. 43 and 49, the EFG tensor and the charge density $\rho(0)$ at the M site.

III. RESULTS AND DISCUSSION

With the method being described in the previous section, we have calculated the electronic structure of the MS_2 series. Orbital occupations, net atomic charges and quadrupole splittings are summarized in Table II. It is interesting to observe that the orbital occupations are very close to the values reported by Bullett,[30] despite the fact that in the former calculations self-consistency was retained only in the diagonal *d* blocks of the Hamiltonian matrix. Calculated and experimental photoelectron spectra are shown in Figs. 1(a) to 1(e). The ratio between the subshell photoionization cross sections has been taken as $\sigma(S_{3s}):\sigma(S_{3p}):\sigma(M_{3d})=4:1:1$ for all elements in the series, while the atomic calculations of Scofield[37] on neutral nickel atoms reveal a ratio of about 4:1:5. To come to a better understanding of the photoelectron intensities it would be desirable to have access to photoelectron cross sections for ions and not only for neutral atoms. In the following we want to discuss our results for the various elements of the MS_2 series.

TABLE II. Band-structure results for the pyrite series MS_2 (M=Fe,Co,Ni,Cu,Zn). The entries in the table are as follows: $Q(M)$ is the net atomic charge at the metal atom M (based on a Mulliken division of overlap charges). $N_{4s}(M)$, $N_{4p}(M)$, $N_{3d}(M)$, N_{3s}(S), and N_{3p}(S) are the orbital populations of the metal and sulfur AO's, respectively; they do not contain any overlap contributions. Calculated and experimental quadrupole splittings at the ^{57}Fe nucleus are given in mm s^{-1}. In CoS_2, NiS_2, CuS_2, and ZnS_2, ΔE_Q has been calculated for low iron concentrations x in $Fe_xM_{1-x}S_2$, and it was assumed that iron has the same electronic configuration as the metal host atom. For comparison ΔE_Q's obtained by MO-cluster calculations on $[M(S_2)_6]^{10-}$ clusters are added in parentheses.

System Configuration of free metal atom	FeS_2 $3d^64s^2$	CoS_2 $3d^74s^2$	NiS_2 $3d^84s^2$	CuS_2 $3d^{10}4s^1$	ZnS_2 $3d^{10}4s^2$
$Q(M)$	0.85	0.65	0.35	0.32	0.80
$N_{4s}(M)$	0.1	0.1	0.1	0.1	0.2
$N_{4p}(M)$	0.2	0.2	0.2	0.3	0.5
$N_{3d}(M)$	6.8	7.9	9.0	9.8	10.0
N_{3s}(S)	2.0	1.9	1.8	1.8	1.8
N_{3p}(S)	4.2	4.1	4.0	3.9	4.2
ΔE_Q^{calc}	−0.74 (−0.89)	−0.23 (−0.76)	−0.24 (−0.62)	−0.07 (−0.55)	0.004 (−0.49)
ΔE_Q^{expt}	0.61[a] +0.62[bc] −0.62[d] −0.65[e]	0.32[f] 0.33[g] −0.34[g] +0.31[c] +0.32[h]	−0.27[h,i]	0.05[j]	

[a]References 12, 14, and 15.
[b]Reference 18.
[c]Reference 20.
[d]Reference 19.
[e]Reference 21.
[f]Reference 16.
[g]Reference 17.
[h]Reference 25.
[i]Reference 26.
[j]Taken from chalcopyrite $CuFeS_2$ [D. Raj, K. Chandra, and S. P. Puri, J. Phys. Soc. Jpn. 24, 39 (1968)].

A. Iron pyrite (FeS_2)

Iron pyrite is a diamagnetic semiconductor with the metal being in the ferrous low-spin state.[13,19] From optical and conductivity measurements various values for the band gap, ranging from 0.84 to 1.2 eV, have been reported.[30] In Fig. 2 the energy dispersion of the bands in FeS_2 along some principal symmetry directions in the Brillouin zone are displayed. This result is in reasonable agreement with the calculations of Bullett,[30] although the bands near the Fermi level are broader in his investigation. Owing to the relatively flat nature of the bands, a relatively small number of quadrature points (about 64) is sufficient to obtain stable results. The bands in FeS_2 can roughly be labeled as indicated in Fig. 2. However, it should be mentioned that except the t_{2g} band all other bands contain significant admixtures from other orbitals. The e_g band, for example, has contributions arising from sulfur p orbitals, resulting in a small antibonding character. Therefore, if one moves through the series from FeS_2 to ZnS_2, it becomes more and more difficult to add another electron into the e_g band. This explains why CuS_2 and ZnS_2 can be synthesized only under high pressure.[8]

In Fig. 1(a) the calculated x-ray photoelectron spectrum (XPS) is compared with two different measurements, and the various structures are labeled according to their origin. The calculation reveals a direct band gap of 0.97 eV and an indirect gap of 0.91 eV, which is in excellent agreement with the values[30] ($\sim$0.9 eV) deduced from experiment.

The imaginary part of the dielectric constant $\epsilon_2(E)$, which is related to transitions from the occupied to the empty bands, is displayed in Fig. 3. The first peak at the low-energy side of the theoretical curve is entirely due to transitions from the Fe t_{2g} to the Fe e_g band, while the remaining structures arise from transitions between the S p bands and the e_g band. All peaks observed in the experimental $\epsilon_2(E)$ curve are resolved in the theoretical curve; there is, however, a slightly too large separation between the first two peaks at low energy in the calculated curve. Since the calculation of $\epsilon_2(E)$ is based on ground-state

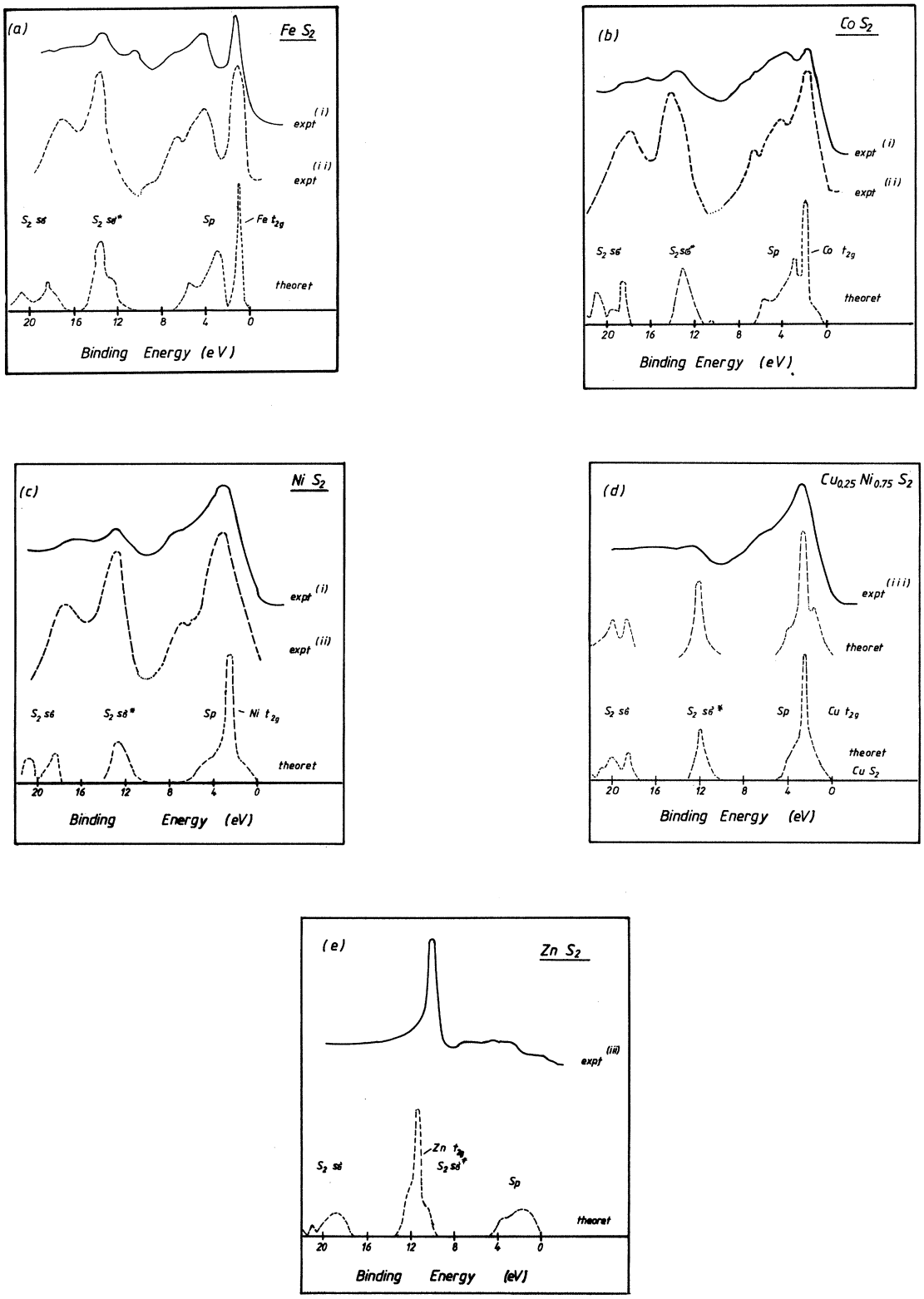

FIG. 1. (a)—(e): Experimental and calculated photoelectron spectra for the MS_2 series. (i) Ref. 2, (ii) Ref. 7, and (iii) Ref. 5.

properties under the condition of Koopman's theorem, electronic relaxation effects during the photoabsorption process could account for the energy shifts required to move the two peaks towards each other. The strong absorption occuring at about 2 eV in the experimental curves could therefore be explained on the basis of an overlapping of $t_{2g} \rightarrow e_g$ and S $p \rightarrow e_g$ transitions.

A great deal of work has been performed to study the

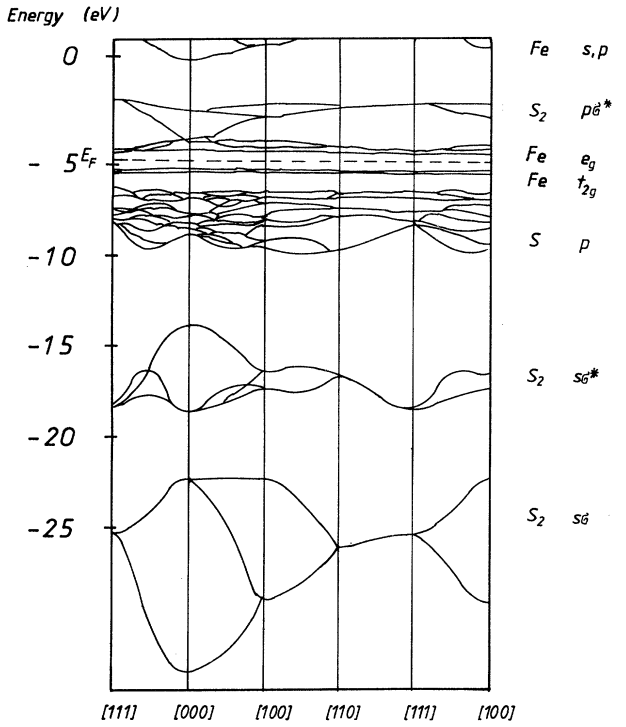

FIG. 2. Theoretical energy dispersion of the electron-energy bands of the pyrite FeS_2 along some principal symmetry directions in the first Brillouin zone.

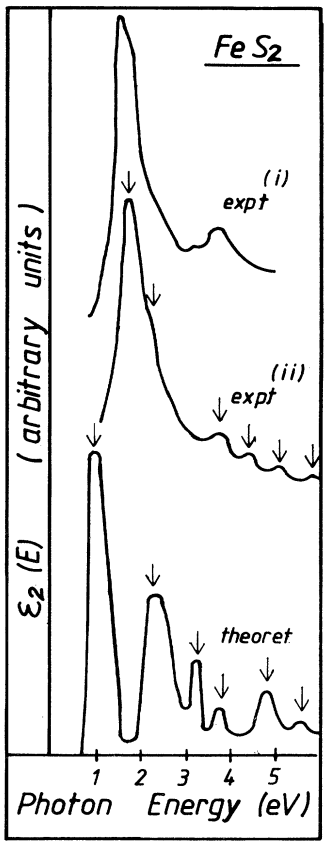

FIG. 3. Experimentally derived and calculated imaginary part of the dielectric constant $\epsilon_2(E)$ for FeS_2. (i) Ref. 8, and (ii) Ref. 9. Curve (i) has been calculated from the complex refractive index $N=n+ik$ of Ref. 8 using the relation $\epsilon_2=2nk$.

local electronic structure at the iron site using Mössbauer spectroscopy.[12,14,15,17–23] Based on point-charge considerations, it was concluded that the EFG tensor primarily arises from the lattice, and not from the distribution of the valence electrons.[18,20,21] The sign of the nuclear-quadrupole coupling constant e^2qQ has been a matter of considerable confusion. Various authors reported a positive sign,[17,18,20] while Montano and Seehra[19] found a negative sign. Other workers then either refer to the one (positive[25,26]) or the other (negative[21,23]) result. We have calculated the EFG tensor at the iron site of FeS_2 using the band-structure method [Eq. (21)] and the MO-cluster approach. We find that ΔE_Q takes the values -0.74 and -0.89 mm s^{-1}, as derived from the band-structure method and the cluster approach, respectively.

Analyzing the contributions to the EFG tensor we find that the dominating term is the valence contribution ($\sim 95\%$) while all other contributions are small. Therefore, it can be justified to separate the EFG tensor into a valence part and a lattice part. In the cubic-axes system the valence contribution arises only from the off-diagonal elements of the "bond-order" matrix elements P_{ij} of the iron block. The diagonal "bond-order" matrix elements P_{ii} of the iron block yield zero contribution on the diagonal of the EFG tensor. For the four iron positions at (0,0,0), $(0,\frac{1}{2},\frac{1}{2})$, $(\frac{1}{2},0,\frac{1}{2})$, and $(\frac{1}{2},\frac{1}{2},0)$ in the primitive unit cell, we find from the band-structure calculation, the following four microscopic EFG tensors:

$$\begin{bmatrix} 0 & A & A \\ A & 0 & A \\ A & A & 0 \end{bmatrix}, \quad \begin{bmatrix} 0 & -A & -A \\ -A & 0 & -A \\ -A & -A & 0 \end{bmatrix},$$
$$\begin{bmatrix} 0 & A & -A \\ A & 0 & -A \\ -A & -A & 0 \end{bmatrix}, \quad \begin{bmatrix} 0 & -A & A \\ -A & 0 & A \\ A & A & 0 \end{bmatrix}, \tag{22}$$

with $A=-0.24a_0^{-3}$. Using the intensity tensor concept of Zimmermann[50] for the calculation of the line intensities in quadrupolar-split Mössbauer spectra, we can associate each of the four microscopic EFG tensors with a microscopic intensity tensor $I_{pq}^{\mathrm{mic}}(i)$ $(i=1,\ldots,4)$. With respect to single-crystal Mössbauer measurements the resultant macroscopic intensity tensor I_{pq}^{mac} is given by a summation over all equivalent microscopic intensity tensors $I_{pq}^{\mathrm{mic}}(i)$ in the unit cell,[50]

$$I_{pq}^{\mathrm{mac}}=\left[\tfrac{1}{4}\sum_{i=1}^{4} I_{pq}^{\mathrm{mic}}(i)\right]+\tfrac{1}{2}\delta_{pq}\ . \tag{23}$$

If an isotropic mean-square displacement tensor is assumed, then the microscopic intensity tensors $I_{pq}^{\mathrm{mic}}(i)$ of Eq. (22) add up to

$$I_{pq}^{\mathrm{mac}}=\tfrac{1}{2}\delta_{pq}\ . \tag{24}$$

With I^h and I^l being the intensity of the high- and low-energy lines of the quadrupolar-split Mössbauer spectrum, respectively, and with e_p and e_q describing the direction cosines of the γ ray with respect to the coordinate system in which I_{pq}^{mac} is given, then the line intensity ratio is given as,[50]

$$\frac{I^h}{I^h+I^l}=\sum_{p,q} I_{pq}^{\text{mac}} e_p e_q \ . \tag{25}$$

An immediate consequence of the form of the intensity tensor given by Eq. (24) is that the line-intensity ratio in Eq. (25) is always $\frac{1}{2}$ and independent of orientation of the γ beam with respect to the single crystal. This was proved experimentally by Guettinger and Williamson[22] and explained by Liu[21] with symmetry arguments. We could verify this now on the ground of electronic structure calculations.

We have extended our theoretical analysis also to the pressure dependence of the EFG tensor of iron pyrite. The experimental data are taken from Vaughan and Drickamer.[14] Calculated quadrupole splittings ΔE_Q and isomer shifts δ are shown in Fig. 4. It can be visualized from this figure that the experimentally observed changes of ΔE_Q and δ as a function of pressure are well accounted for by the theoretically derived electronic structure. Vaughan and Drickamer[14] explained the pressure-induced changes of ΔE_Q and δ as only being due to the change of lattice contributions, while we find that both lattice and valence contributions are almost equal in importance when explaining the pressure-induced changes.

B. Cobalt pyrite (CoS_2)

The calculations on the ferromagnetic metal, cobalt pyrite, have been performed assuming four unpaired spins per primitive unit cell. Calculated and experimental photoelectron spectra are shown in Fig. 1(b). Similar as in Bullett's[30] calculation we have found that the t_{2g} levels in CoS_2 move downwards to lower energies by about 1.1 eV (0.9 eV in Ref. 30) as compared to FeS_2. The bandwidth of the e_g state is about 0.6 eV.

In Fig. 5 the imaginary part of the dielectric constant is displayed. The large absorption occurring at low energies (<1 eV) is entirely due to transitions from occupied e_g states into empty e_g states, while the small peak at 1.3 eV arises from transitions $t_{2g}\rightarrow e_g$. The broad structure between 3 and 5 eV is associated with transitions from the S p band to the empty e_g levels. With these findings the structures found in the experimentally derived $\epsilon_2(E)$ curve can be assigned.

Solid solutions of iron in CoS_2 have been also studied by means of Mössbauer Spectroscopy.[16,17,20,24,25] For low Fe concentrations, a quadrupole splitting of about 0.32 mm s^{-1} has been found. As in FeS_2 the sign of the coupling constant e^2qQ has not been clearly resolved. Woodhams *et al.*[17] demonstrated that their spectra can be fitted by either sign. Wortman *et al.*[24] resolved a positive sign using an external magnetic field of 6 T. However, an ex-

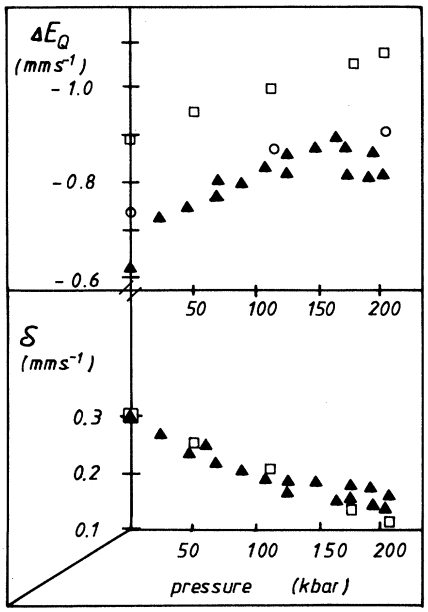

FIG. 4. Quadrupole splitting ΔE_Q and isomer shift δ in the pyrite FeS_2 as a function of pressure. Solid triangles refer to the experimental values of Vaughan and Drickamer (Ref. 14), open squares arise from MO-cluster calculations on a $[Fe(S_2)_6]^{10-}$ cluster, and open circles are the result of band-structure calculations.

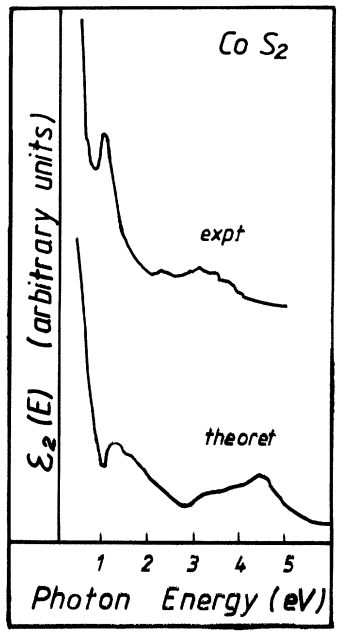

FIG. 5. Experimental and calculated imaginary part of the dielectric constant $\epsilon_2(E)$ for CoS_2. The experimental curve was derived from the complex refractive index $N=n+ik$ of Ref. 8 using the relation $\epsilon_2=2nk$.

trapolation to zero magnetic field does not seem to be justified in this case, because the system reveals a large magnetically induced quadrupole splitting. Ward and Howard[20] found, on the basis of point-charge calculations, a positive sign. However, the valence contribution, which turned out to be the dominating term in FeS_2, was completely neglected in their study. McCann and Ward[25] concluded a positive sign; however, their fits with positive and negative sign, respectively, hardly show any differences.

We have calculated the EFG tensor at the iron site in the solid solutions $Fe_xCo_{1-x}S_2$ with concentrations $x=0.01$, 0.25, 0.5, and 0.75. Structural data and experimental quadrupole splittings have been taken from Gallagher *et al.*[16] Since our band-structure program does not allow the handling of low Fe concentrations ($x=0.01$) we have assumed instead that, for low concentrations, iron has the same electronic structure as a cobalt atom. For all other concentrations one, two or three cobalt atoms in the primitive unit cell have been replaced by iron. In the order of ascending Fe concentration we have calculated ΔE_Q to be -0.23 mm s^{-1} (0.32 mm s^{-1}; $x=0.01$), -0.47 mm s^{-1} (0.40 mm s^{-1}; $x=0.25$), -0.70 mm s^{-1} (0.54 mm s^{-1}; $x=0.5$), and -0.71 mm s^{-1} (0.54 mm s^{-1}; $x=0.75$), where the values in parentheses refer to the experimental results of Gallagher *et al.*[16] As in FeS_2, the EFG arises in the isostructural CoS_2 primarily from the valence contribution, and e^2qQ is negative.

The magnetic hyperfine field at the iron nucleus in $Fe_xCo_{1-x}S_2$, with low concentrations x, was found to range from -0.6 to -1.0 T;[17,24] the minus sign here means that the hyperfine field at the iron nucleus is opposite in direction to the magnetization of the cobalt sublattice. For $Fe_{0.25}Co_{0.75}S_2$, we have calculated the amount of unpaired spin density in the $4s$ and $3d$ orbitals of iron from the band-structure results. These spin densities originate only from small admixtures of Fe orbitals in the e_g bands of cobalt and should not be mixed up with supertransferred spin densities.[49] Estimating the effect of spin polarization of the iron-core s orbtials via the $3d$ spin along the lines described in Ref. 49 and 51, the contact field is found to be $B^c(3d)=-1.0$ T, while the direct contribution of the $4s$ spin yields $B^c(4s)=0.3$ T. The total B^c then takes the value -1.6 T. Each of the six nearest-neighbor sulfur atoms carries, due to covalency, a small spin density on the order of 0.03. This will give rise to an additional supertransferred field,[52] which will be positive (e.g., the same direction as the cobalt sublattice magnetization) and will therefore yield a somewhat smaller hyperfine field compared to $B^c=-1.6$ T.

C. Nickel, copper, and zinc pyrite (NiS_2, CuS_2, and ZnS_2)

Experimental and calculated photoelectron spectra for the pyrites NiS_2 and ZnS_2 are displayed in Figs. 1(c)–1(e). It is observed that the metal d states continuously move through the sulfur p bands as we proceed in the series to ZnS_2. NiS_2 is characterized as a Mott semiconductor,[53] while CuS_2 exhibits metallic character and a weak Pauli paramagnetism.[1] Finally, zinc pyrite, ZnS_2, is a semiconductor, again with a completely filled d band. From the bright yellow color[8] it was estimated[30] that the band gap should be on the order of 2.5 eV. This is in agreement with our calculation which shows a direct band gap of 2.7 eV. Calculated quadrupole splittings at the iron site in solid solutions of iron in NiS_2, CuS_2, and ZnS_2 in the low-concentration limit are summarized in Table II. As in CoS_2 it was assumed that iron has the same electronic environment as the host metal atom. While the nuclear-quadrupole coupling constant e^2qQ was calculated to be negative in NiS_2 and CuS_2, a positive sign was found in ZnS_2. This arises because in the d^{10} system ZnS_2 only the positive lattice contribution to the EFG tensor is left. Zinc Mössbauer spectroscopy would be extremely useful to check this statement experimentally. Unfortunately, no experimental results are available for ZnS_2 so far. However, if the calculated quadrupole splitting is compared with the results obtained for ZnS [$\Delta E_Q^{\text{expt}}\sim 0.0$ (Ref. 54)], reasonable agreement is obtained.

IV. CONCLUSIONS

Using a semiempirical and self-consistent LCAO tight-binding method we have calculated the electronic structure of the pyrite series MS_2 (M=Fe, Co, Ni, Cu, Zn). The results obtained are in reasonable agreement with the recent band-structure investigation of Bullett, where self-consistency was retained only in the diagonal d blocks of the Hamiltonian matrix. Photoelectron intensities have been calculated, and it was found that the theoretically derived photoelectron cross sections for neutral atoms cannot account for the observed intensities. From calculations of the imaginary part of the dielectric constant $\epsilon_2(E)$ in FeS_2 and CoS_2, the structures found in experimental studies could be assigned to appropriate transitions. Evidence was found that the strong absorption at about 2 eV in FeS_2 is due to a superposition of $t_{2g}\rightarrow e_g$ and S $p\rightarrow e_g$ transitions. The ^{57}Fe Mössbauer parameters have been calculated in FeS_2 and Fe-doped MS_2 (M=Co, Ni, Cu, Zn). The pressure dependence of ΔE_Q in FeS_2, as well as the concentration dependence of ΔE_Q in the solid solutions $Fe_xCo_{1-x}S_2$ ($x=0.01,0.25,0.5,0.75$), was investigated. These studies yielded that, except in ZnS_2, the sign of the nuclear-quadrupole coupling constant e^2qQ is negative. The EFG tensor in FeS_2 primarily arises from a nonspherical distribution of electrons in the metal valence shell, while the lattice contribution to the EFG is small and positive. Proceeding from FeS_2 to ZnS_2, the valence contribution continuously decreases, and in the d^{10} system ZnS_2 only the small and positive lattice EFG is left.

MO-cluster calculations have been performed on $[MS_6]^{4-}$ clusters, but convergence could not be achieved properly. However, the use of $[M(S_2)_6]^{10-}$ clusters yields results which are in reasonable agreement with the band-structure calculations and with experiment. It is therefore concluded that the use of the S_2-anion pairs is extremely important for MO-cluster calculations in the pyrite system. Especially local properties at the metal site [such as the EFG tensor and the charge density $\rho(0)$ at the nuclear site of ^{57}Fe] can be obtained by choosing appropriate cluster size and symmetry.

ACKNOWLEDGMENT

This work was supported partly by the North Atlantic Treaty Organization (NATO, Grant No. 1606). The computer work was performed at the Rechenzentrum der Universität des Saarlandes and at the Department of Physics, University of Utah. Two of the authors (S. L. and A. X. T.) want to express their gratitude to Professor U. Gonser for making it possible to perform most of the present work in his laboratory in Saarbrücken.

[1]J. A. Wilson and A. D. Yoffee, Adv. Phys. 18, 193 (1969).
[2]A. Oshawa, H. Yamamoto, and H. Watanabe, J. Phys. Soc. Jpn. 37, 568 (1974).
[3]E. K. Li, K. H. Johnson, D. E. Eastman, and J. L. Freeouf, Phys. Rev. Lett. 32, 470 (1974).
[4]U. Berg, G. Dräger, K. Mosebach, and O. Brümmer, Phys. Status Solidi B 75, K89 (1976).
[5]H. Yamamoto, T. Nakagawa, H. Onodera, and H. Watanabe, J. Phys. Soc. Jpn. 43, 1095 (1977).
[6]D. Brion, Appl. Surf. Sci. 5, 133 (1980).
[7]H. van der Heide, R. Hemmel, C. F. van Bruggen, and C. Haas, J. Solid State Chem. 33, 17 (1980).
[8]T. A. Bither, R. J. Bouchard, W. H. Cloud, P. G. Donohue, and W. J. Siemons, Inorg. Chem. 7, 2208 (1968).
[9]A. Schlegel and P. Wachter, J. Phys. C 9, 3363 (1976).
[10]W. W. Kou and M. S. Seehra Phys. Rev. B 18, 7062 (1978).
[11]M. S. Seehra and S. S. Seehra, Phys. Rev. B 19, 6620 (1979).
[12]A. A. Temperley and H. W. Lefevre, J. Phys. Chem. Solids 27, 85 (1966).
[13]S. Miyahara and T. Teranishi, J. Appl. Phys. 39, 896 (1968).
[14]R. W. Vaughan and H. G. Drickamer, J. Chem. Phys. 47, 468 (1967).
[15]D. Raj and S. P. Puri, Nuovo Cimento 2B, 261 (1969).
[16]P. K. Gallagher, J. B. MacChesney, and R. G. Sherwood, J. Chem. Phys. 50, 4417 (1969).
[17]F. W. D. Woodhams, P. S. White, and O. Knop, J. Chem. Phys. 5, 334 (1972).
[18]V. K. Garg, Y. S. Liu, and S. P. Puri, J. Appl. Phys. 45, 70 (1974).
[19]P. A. Montano and M. S. Seehra, Solid State Commun. 20, 897 (1976).
[20]J. B. Ward and D. G. Howard, J. Appl. Phys. 47, 388 (1976).
[21]Y. S. Liu, Phys. Rev. B 20, 71 (1979).
[22]T. W. Guettinger and D. L. Williamson, Phys. Rev. B 20, 3938 (1979).
[23]V. K. Garg, J. Appl. Phys. 52, 373 (1981).
[24]G. Wortmann, N. S. Ovanesyan, V. A. Trukhtanov, and N. I. Bezmen, Zh. Eksp. Teor. Fiz. 69, 2093 (1975) [Sov. Phys.—JETP 42, 1064 (1975)].
[25]V. H. McCann and J. B. Ward, J. Phys. Chem. Solids 38, 991 (1977).
[26]Y. Nishihara, S. Ogawa, and S. Waki, J. Phys. Soc. Jpn. 39, 63 (1975).
[27]J. A. Tossel, J. Chem. Phys. 66, 5712 (1977).
[28]J. A. Tossel, D. J. Vaughan, and J. K. Burdett, *Physics and Chemistry of Minerals* (Springer, Berlin, 1981), Vol. 7, p. 177.
[29]M. H. Khan, J. Phys. C 9, 81 (1976).
[30]D. W. Bullett, J. Phys. C 15, 6163 (1982).
[31]V. R. Marathe, S. Lauer and A. Trautwein, Phys. Status Solidi B 100, 149 (1980).
[32]L. C. Cusachs, J. Chem. Phys. 43, S 157 (1965).
[33]C. E. Moore *Atomic Energy Levels,* National Bureau of Standards Circular No. 467 (U. S. GPO, Washington, D. C., 1952).
[34]V. R. Marathe, S. Lauer, and A. Trautwein, Phys. Rev. B 27, 5162 (1983).
[35]M. Grodzicki, J. Phys. B 13, 2683 (1980).
[36]U. Gelius, in *Electron Spectroscopy,* edited by D. A. Shirley (North-Holland, Amsterdam, 1972), p. 311.
[37]J. H. Scofield, J. Electron Spectrosc. Relat. Phenom. 8, 129 (1976).
[38]S. M. Goldberg, C. S. Fadley, and S. Kono, J. Electron Spectrosc. Relat. Phenom. 21, 285 (1981).
[39]M. Cardona and L. Ley, in *Photoemission in Solids I,* edited by M. Cardona and L. Ley (Springer, Berlin, 1978), p. 82.
[40]G. Harbeke, in *Optical Properties of Solids,* edited by F. Abelés (North-Holland, Amsterdam, 1976), p. 23.
[41]R. M. Sternheimer, Phys. Rev. A 6, 1702 (1972).
[42]S. Lauer, V. R. Marathe, and A. Trautwein, Phys. Rev. A 19, 1852 (1979).
[43]M. Grodzicki, S. Lauer, A. Trautwein, and A. Vera, in *Mössbauer Spectroscopy and Its Chemical Applications (Advances in Chemistry Series 194),* edited by J. G. Stevens and G. K. Shenoy (American Chemical Society, Washington, D. C., 1981), p. 1.
[44]M. Abramowitz and I. Stegun, *Handbook of Mathematical Functions* (Dover, New York, 1965), p. 916.
[45]H. J. Monkhorst and J. D. Pack, Phys. Rev. B 13, 5188 (1976).
[46]A. H. McDonald, Phys. Rev. B 18, 5897 (1978).
[47]W. R. Fehlner, S. B. Nickerson, and S. H. Vosko, Solid State Commun. 19, 83 (1976).
[48]A. Trautwein and F. E. Harris, Theor. Chim. Acta 30, 45 (1973).
[49]H. Winkler, R. Eisberg, E. Alp, R. Rüffer, E. Gerdau, S. Lauer, A. X. Trautwein, M. Grodzicki, and A. Vera, Z. Phys. B 49, 331 (1983).
[50]R. Zimmermann, Nucl. Instrum. Methods 128, 537 (1975).
[51]V. R. Marathe and A. Trautwein, in *Advances in Mössbauer Spectroscopy,* Vol. 25 of *Studies in Physical and Theoretical Chemistry,* edited by B. V. Tosar, P. K. Iyengar, J. K. Srivastava, and S. C. Bhargava (Elsevier, New York, 1983), p. 398.
[52]G. A. Sawatzky and F. van der Woude, J. Phys. (Paris) Colloq. 35, C6-47 (1974).
[53]S. Endo, T. Mitsui, and T. Miyadai, Phys. Lett. 46A, 29 (1973).
[54]A. Forster, W. Potzel, and G. M. Kalvius, Z. Phys. B 37, 209 (1980).